Journal of Nuclear Materials 378 (2008) 9–16

Contents lists available at ScienceDirect

Journal of Nuclear Materials

journal homepage: www.elsevier.com/locate/jnucmat

Pitting corrosion in CVD SiC at 300 °C in deoxygenated high-purity water

Charles H. Henager Jr. *, Alan L. Schemer-Kohrn, Stan G. Pitman, David J. Senor, Kenneth J. Geelhood, Chad L. Painter

Materials Science Division, Pacific Northwest National Laboratory, P.O. Box 999, Richland, WA 99336, USA

ARTICLE INFO

Article history:
Received 11 July 2007
Accepted 18 March 2008

PACS:
81.05.Je
81.65.Mq
87.64.Ee
82.45.Bb

ABSTRACT

SiC is a candidate for nuclear applications at elevated temperatures but has not been fully studied under typical light-water reactor operating conditions, such as moderate temperatures and high pressures. Coupons of high-purity chemical vapor deposited SiC were exposed to deoxygenated, pressurized water at 573 K and 10 MPa for up to 5400 h. Ceramographic examination of the exposed SiC surfaces revealed both embryonic and large, $d > 300$ μm, pits on the surface after initial exposure for 4000 h. The pits were characterized using scanning electron microscopy for structure and chemistry analysis. Pit densities were also determined by standard counting methods. The chemical analysis revealed that the pits are associated with the formation of silica and subsequent loss of Si, which is expected due to several suggested reactions between SiC and water. Subsequent exposure under nominally identical water chemistry conditions for an additional 1400 h removed the pits and the samples exhibited general corrosion with measurable loss of Si from the surface.

1. Introduction

Beta-silicon carbide, β-SiC, is a material of great interest for many nuclear applications because it is strong, temperature resistant, corrosion resistant, low-activation, and radiation damage resistant relative to metals and other ceramics [1–5]. Its properties suggest an optimal use temperature of about 1373 K in a high-purity helium or dry gas environment, such as for high-temperature gas-cooled reactor concepts. The 1373 K-use temperature is suggested by the minimum in the swelling curve for β-SiC [6,7]. The need for dry inert environment is suggested by the sensitivity of silicon-containing ceramics to oxygen and water vapor corrosion [8–13]. β-SiC, which is cubic, compares favorably to graphite for these applications due to its much-improved radiation damage resistance, greater oxidation resistance, and much higher mechanical strength. Ceramic composites can be engineered for increased fracture toughness to overcome the brittle fracture behavior of monolithic SiC [14,15].

Although the interest in β-SiC is not restricted to high-temperature, gas-cooled reactors operating at elevated temperatures, the limitations of SiC need to be understood in the context of other nuclear applications so that new and innovative concepts can be safely and thoughtfully brought to the design stage [1,2]. In this context, β-SiC has two shortcomings that require greater attention so that proper use of this important material can be realized. One of the main shortcomings of β-SiC for uses other than as stated above are the temperature-dependent swelling that increases as the use temperature decreases below the temperature where point defect recombination occurs [7]. The other shortcoming is the rather unfortunate lack of corrosion resistance of SiC in water and water vapor due to the formation of stable silicon hydroxides, even at low temperatures [8–13]. The swelling data is rather complete for β-SiC in the temperature range of 300–1730 K [6,7]. But, corrosion data of high-purity β-SiC in water is somewhat lacking for temperatures in the vicinity of 573 K, the operating temperatures of many water-cooled reactors [16–19].

Corrosion of SiC hinges on the corrosion resistance and environmental stability of the main condensed corrosion product, SiO_2. The degradation of silicon-containing ceramics in water vapor, both static and flowing, has been extensively studied and appears to be well understood, and unfortunate [8–13]. The formation of volatile silicon hydroxides that are non-protective is at the root of this corrosion. Similarly, the degradation of SiO_2, usually in the form of silica glass, has been well studied for the cases of stress-corrosion of glasses and optical fibers [20–25]. Again, silicon hydroxides are involved but also the interdiffusion of water into silica and the enhanced reaction rates due to strain are major issues in the stress corrosion and degradation of silica glass. The corrosion resistance of SiC in water, since silica films are involved, is expected to be reliant on similar chemistry issues. This research fills in a bit of a gap in the available data for β-SiC corrosion in water at 573 K by exposure of high-purity materials in water conditions suitable for a pressurized water reactor.

* Corresponding author.
E-mail address: chuck.henager@pnl.gov (C.H. Henager Jr.).

0022-3115/$ - see front matter © 2008 Elsevier B.V. All rights reserved.
doi:10.1016/j.jnucmat.2008.03.025

Table 1
Chemistry of the deoxygenated water used in these tests

Chemistry data	Value
pH	4.6
O_2	<10 appb
F^-	<0.08 appm
Cl^-	<0.1 appm
NO_2^-	<0.1 appm
NO_3^-	<0.2 appm
PO_4^{-3}	<0.3 appm
SO_4^{-2}	<0.4 appm
CrO_4^{-2}	<0.4 appm
Si	<0.004 appm

2. Experimental

Coupons of ultra high-purity chemical vapor deposited (CVD) β-SiC,[1] >99.9995% SiC, were prepared from plate stock by machining and polishing to better than 1 μm diamond finish (one surface). Samples were thoroughly cleaned in ethanol, dried, and weighed to the nearest 0.0001 g. High-pressure autoclaves were prepared with water chemistries according to Table 1 so that the SiC samples could be immersed in the water at 573 K and 10 MPa pressure. In particular, purging with high-purity argon, deoxygenated high-purity water having oxygen levels less than 10 ppb O_2, nominally 18 megohm cm, and a hydrogen overpressure of 140 kPa was applied to match current trends in dissolved oxygen control in nuclear power plants [26]. The deoxygenated water was pumped through the autoclave at a low flow rate in a once-through mode. Typical composition of the water is given in Table 1. Water chemistry was determined using an ion chromatograph and an inductively coupled argon plasma-optical emission spectrometer. Samples were exposed for 2000 and 4000 h, examined using optical and electron microcopy, exposed for an additional 1400 h each and examined a second time in the same manner. After exposures the coupons were weighed and examined in an optical microscope and in a scanning electron microscope (SEM) equipped with energy dispersive spectroscopy (EDS) and operated at 25 kV in secondary and backscatter imaging modes. Surface roughness of the exposed and control samples was measured using a Dektak stylus profilometer with a 12.5 μm radius stylus and using a 2000 μm scan length to find average arithmetic average surface roughness, but only after the final exposure.

3. Results

Measured weight changes for the β-SiC coupons were zero within uncertainty after 5400 h of exposure. Longer exposure times or smaller samples would be required to obtain any kinetic information using weight change data, but other techniques, such as IR spectroscopy, which were not used in this study, may be able to provide information related to reaction kinetics for future studies. However, surface microstructural changes were observed after 2200 and 4000 h using optical microscopy and surface pitting and inhomogeneous chemical changes were observed in the SEM that provide information that suggests the form of chemical attack that is occurring. The additional 1400 h exposure removed the pits but overall surface degradation and roughening was noted with loss of Si relative to the control sample measured using semi-quantitative EDS techniques.

3.1. Optical microscopy

Reflected light microscopy with diffuse lighting was used to image the surfaces of the highly polished coupons. Fig. 1 shows low

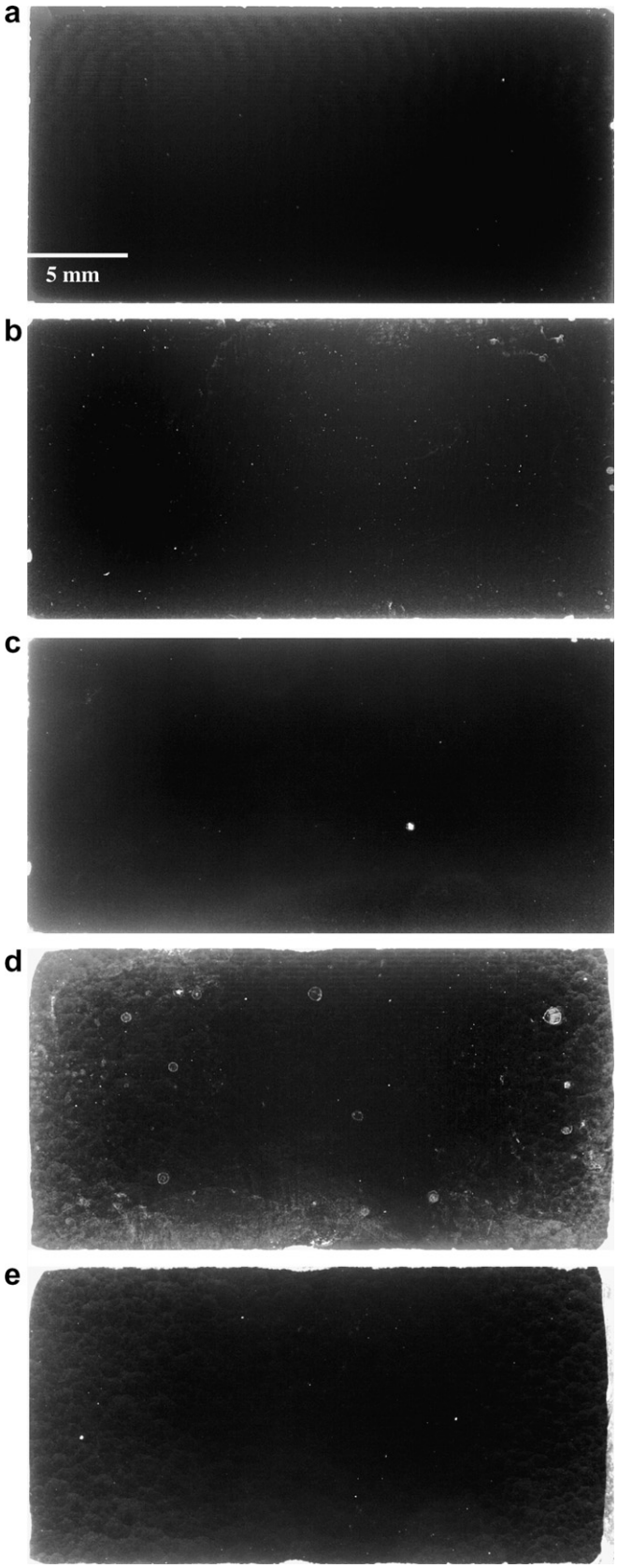

Fig. 1. Optical micrographs taken in diffuse light showing (a) as-polished surface, (b) SiC#5 2200 h exposure, (c) SiC#5 with additional 1400 h re-exposure for total of 3600 h exposure, (d) SiC#3 4000 h exposure, and (e) SiC#3 additional 1400 h re-exposure for total of 5400 h exposure. The pits are observed as bright circular regions in these photos.

[1] Rohm & Haas Company Advanced Materials, Woburn, MA 01801.

magnification (~10×) optical photographs of the β-SiC coupon surfaces as polished, SiC#5 with 2200 h and 3600 h exposure times, and SiC#3 with 4000 h and 5400 h exposure times, respectively. No pits are observed on the as-polished surface while several pits are seen in both of the exposed coupons after their initial exposures of 2200 h and 4000 h, with the 4000 h coupon, SiC#3, showing the largest pits. A pit density was estimated from these photos by direct counting on the polished surfaces to be $1.5 \times 10^6\ m^{-2}$ for both samples exposed to the 573 K pressurized water for 2200 h and 4000 h, respectively. Several of the larger pits and some other surface features from SiC#5 2200 h exposure specimen are shown in optical micrographs in Fig. 2. After an additional 1400 h exposure the pits were no longer visible on the surface of either SiC#5 3600 h or SiC#3 5400 h exposed sample as shown in Fig. 1(c) and 1(e). The surface appears dull as compared to the as-polished control sample but the pits that were easily observed in the early exposures are absent.

3.2. Scanning electron microscopy of pits

Imaging and chemical analysis of the pits, exposed but unpitted surfaces, and control surfaces were performed to determine pit structure and composition, general surface compositional effects, and overall morphological changes. The EDS X-ray data clearly indicate a general loss of Si from the surface after exposure and after the initial exposure this data indicates a high degree of inhomogeneity in the surface composition that gives way at longer times to a more uniform surface corrosion and loss of Si.

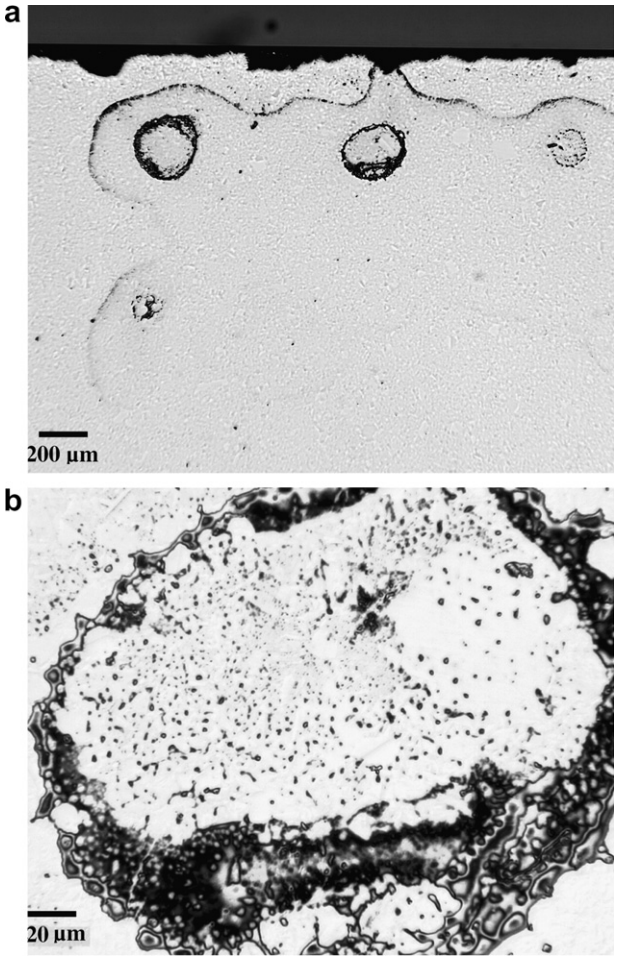

Fig. 2. Optical micrographs of SiC#5 2200 h exposure using reflected light showing (a) four larger pits near the sample edge together with an undulating corrosion front and (b) the middle of the three pits shown in (a). The higher magnification photo shows that the large pits involve hundreds of smaller corrosion pits.

The large pits observed in the 2200 h and 4000 h exposure times are apparently a region of active corrosion comprised of thousands of smaller corrosion pits, which are not resolved in optical microscopy. The structure of the pits can be characterized as a fractal-like arrangement many of active corrosion centers with composition variations showing typically lower Si:C ratios compared with the as-polished material. Fig. 3 shows the fractal-like structure of a large pit on the SiC#3 4000 h exposed sample with the image taken using secondary electron mode. The darker regions correspond to C-rich regions or regions where Si was dissolved (see below). Although the pit itself is about 400 μm in diameter, the smallest features surrounding the pit are nearly circular submicron regions. The underlying grain structure of the β-SiC is visible and it is apparent that the smallest features are associated with grain boundaries or are aligned with the underlying texture of the grains as shown in Fig. 3(e) and (f).

Energy dispersive spectroscopy (EDS) was used to perform compositional profiles of several smaller pits via direct X-ray mapping. In addition, several point spectra were obtained in various regions associated with the pits. In all cases, the pit is a region of reduced Si:C ratio suggesting either C deposition or, more likely, Si dissolution. The average Si:C atomic ratio determined from the as-polished control sample using EDS was 49.4:50.3 with a small amount of oxygen in some locations. The average ratio on the exposed surface of the 2200 h and 4000 h samples was 48.5:51.4 and 39.3:57.8, respectively. The point spectra taken for several pits and the average surface data are shown in Table 2 for the exposed and control samples. Fig. 4 shows a typical X-ray map of one of the smaller pits that correlates the pit morphology and contrast in the SEM with compositional information. The dark contrast region is associated with Si depletion, C enrichment, and presence of O. Fig. 5 is a plot of the average Si content as a function of location on the surface and as a function of exposure time showing the dramatic loss of Si on the surface and in the pit interiors due to dissolution for the 2200 h and 4000 h exposure samples with the pits. The carbon data is not shown from Table 2 in this plot but it essentially mirrors the Si loss with C increases relative to stoichiometric SiC.

3.3. Scanning electron microscopy of un-pitted surfaces

Although samples exposed an additional 1400 h did not have pits the surfaces were examined using some of the same tools in order to observe critical differences due to the water exposure. Fig. 6 shows typical surfaces of the control, 3600 h, and 5400 h exposed samples, respectively. The surface of the specimen exposed for 5400 h appears rough in comparison to the unexposed sample and the visible grain structure in Fig. 6(a) and (b) appears distorted in (c). Surface compositional information was obtained using EDS as before and this is shown in Fig. 7, including that average surface data obtained from all the samples. The data clearly indicate a loss of Si from the surface with increasing exposure time. Sample #3 shows a reversal in the trend after 5400 h compared to 4000 h due to the second exposure during which time the pits vanished from the surface.

3.4. Surface roughness

Following the final exposure testing and after examination of the SEM surface micrographs of SiC Sample #3 surface roughness measurements were performed using a stylus profilometer equipped with a 12.5 μm radius stylus and automated software for computing average arithmetic roughness, Ra. These data are

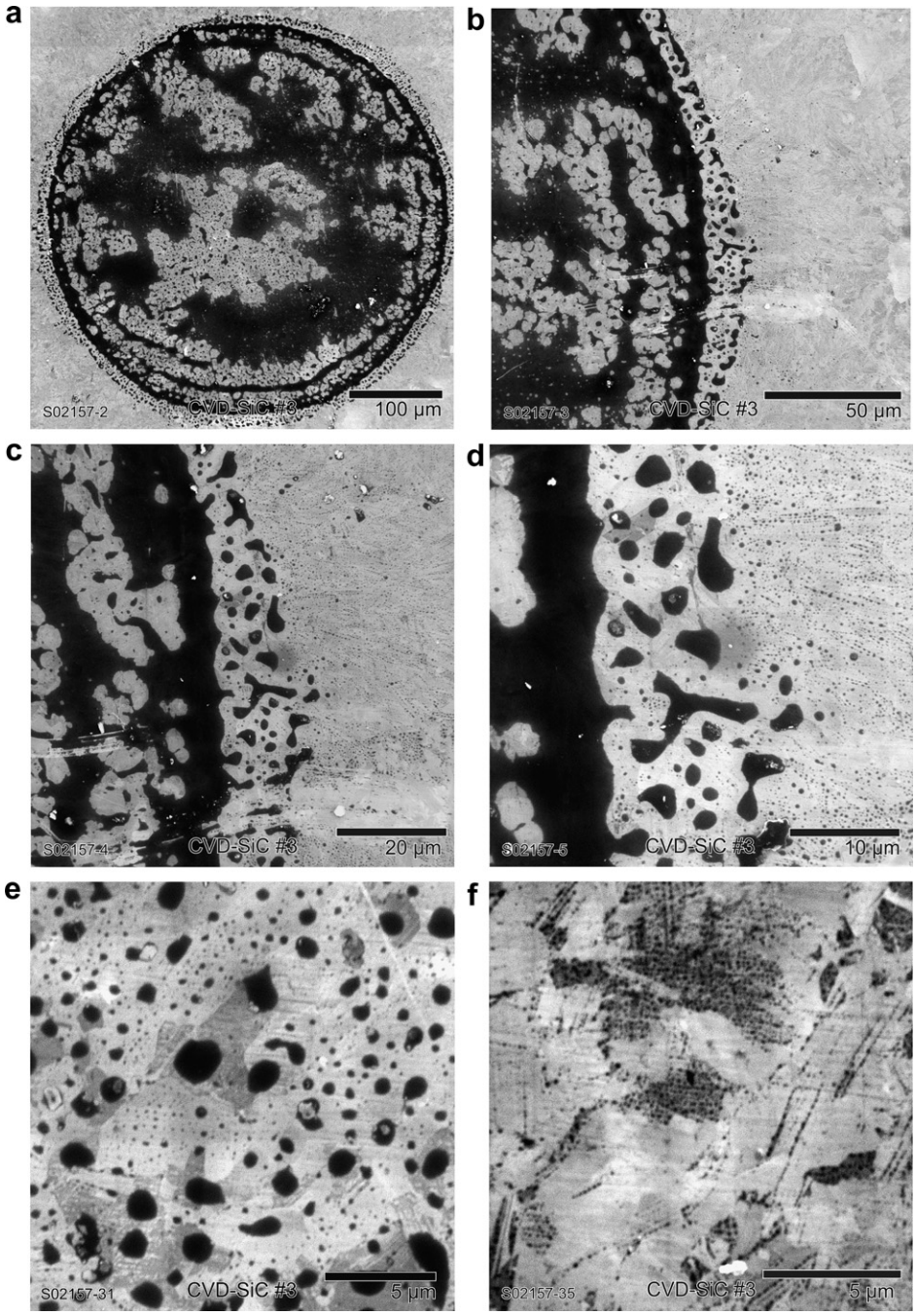

Fig. 3. SEM images of large pit on SiC#3 4000 h exposure showing complex fractal-like pit morphology in (a)–(d). The smallest features surrounding the large pit are submicron and appear to be associated with the underlying microstructural features (d)–(f). The small pits are aligned within individual grains in (f).

Table 2
Si, C, O compositions of pits, pit edges, and exposed surfaces from EDS data

Specimen	Pit or surface description	Location	Si (at.%)	C (at.%)	O (at.%)
As Polished	Polished surface	Surface without pit	49.2 ± 0.4	50.6 ± 0.5	0.0
SiC-2200 h exposure	Oxidized surface	Surface without pit	48.5 ± 1.0	51.4 ± 1.2	0.0
SiC-4000 h exposure	Oxidized surface	Surface without pit	39.3 ± 6.0	57.8 ± 1.5	2.8 ± 2.5
SiC-2200 h exposure	Pit interior, black region	Interiors of several pits	43.6 ± 9.1	53.6 ± 3.9	2.8 ± 2.5
SiC-4000 h exposure	Pit interior, black region	Interiors of several pits	33.1 ± 3.7	65.8 ± 3.5	1.2 ± 1.0
SiC-2200 h exposure	Pit transition region	Edges of several pits	46.9 ± 2.4	52.4 ± 1.9	0.7 ± 0.5
SiC-4000 h exposure	Pit transition region	Edges of several pits	44.0 ± 3.2	55.6 ± 3.5	0.4 ± 0.2
SiC-3600 h exposure	Oxidized surface	Surface in typical region	48.8 ± 1.6	51.0 ± 1.6	0.2 ± 0.2
SiC-5400 h exposure	Oxidized surface	Surface in typical region	45.9 ± 3.9	53.7 ± 3.8	0.4 ± 0.2

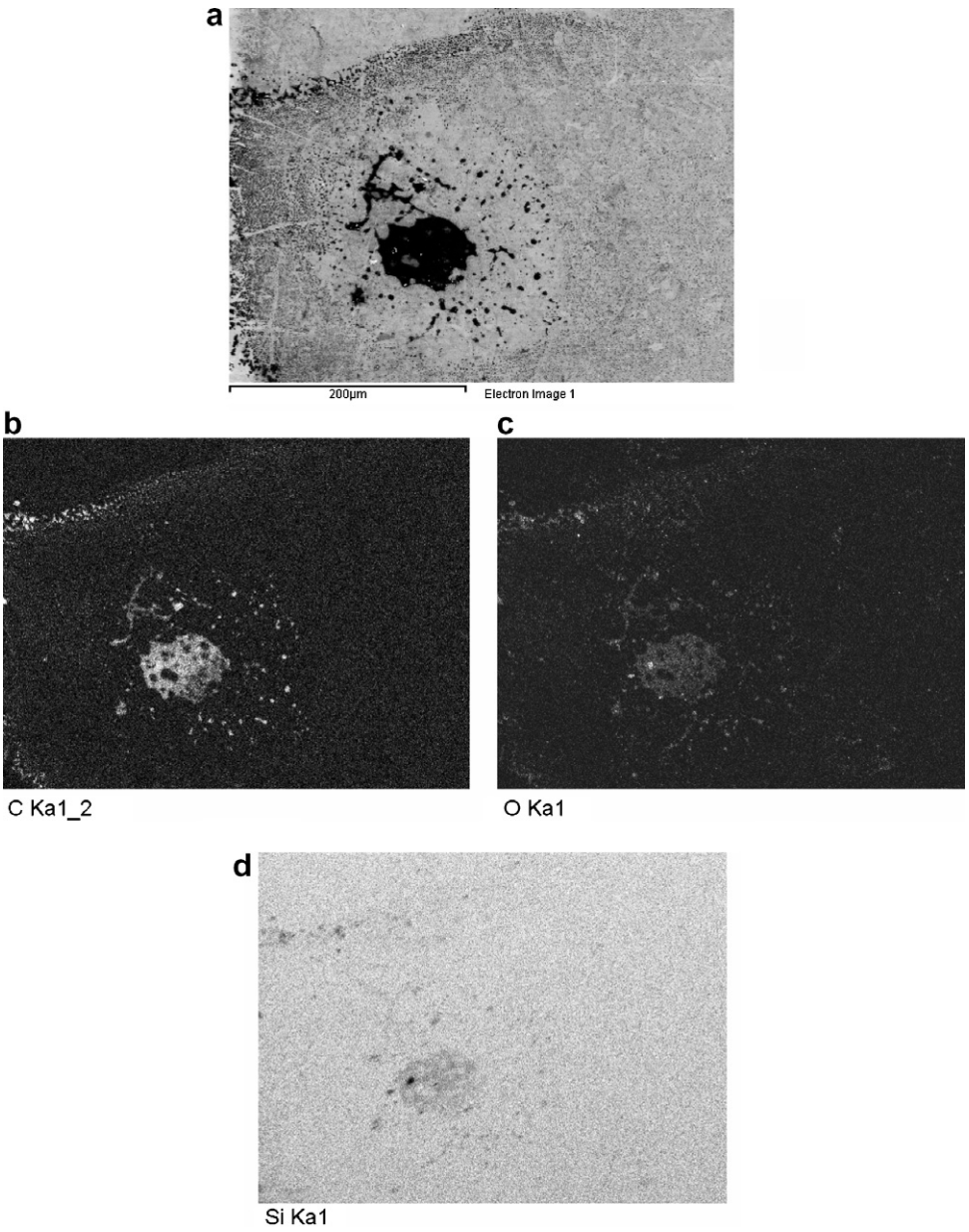

Fig. 4. SEM image and X-ray map images of a pit on the 2000 h exposed sample. The image in (a) can be directly correlated with the associated element maps shown in (b)–(d). The carbon map is shown in (b), the oxygen map in (c) and the silicon map in (d). The pit is enriched in C and O relative to the matrix and depleted in Si.

shown in Fig. 8 for the as-polished and exposed samples using six runs per sample and a scan length of 2000 µm. The scans were performed in both the longitudinal and transverse orientations relative to the specimen axes to minimize systematic errors. The results for the average of the six roughness scans for each sample is shown in Fig. 8 and the data indicate a gradual roughening of the surface with increase exposure.

4. Discussion

Hirayama et al. exposed α-SiC to oxygenated and de-oxygenated water at 563 K and documented mass loss and surface corrosion after 3–200 h exposures in static conditions [17]. Surface etching of grain boundaries and pores was observed along with either linear mass loss under slightly acidic pH or parabolic mass loss under slightly basic pH conditions. Mass loss was greatest for oxygenated water compared to de-oxygenated water conditions and the inability of α-SiC to form SiO_2 under these conditions was discussed and rationalized by the formation of soluble silicon hydroxides. The research of Tomozawa and Doremus on the chemistry of silica in water is relevant here in identifying water–silica reactions [20–25].

Kim et al. exposed CVD β-SiC to static distilled water at 633 K for up to 240 h and observed parabolic mass loss and preferential surface corrosion along CVD columnar grain boundaries [16,19]. Mass loss was higher for SiC containing free Si compared to higher purity CVD SiC and it was hypothesized that similar surface dissolution of silicon via soluble hydroxides was occurring as for Hirayama et al. [17]. A similar study using reaction-bonded SiC (RBSC) found much higher corrosion rates for RBSC compared to CVD SiC at 633 K [19].

Barringer et al. [18] exposed high-purity CVD β-SiC, from the same source as for this work, to de-oxygenated flowing water at

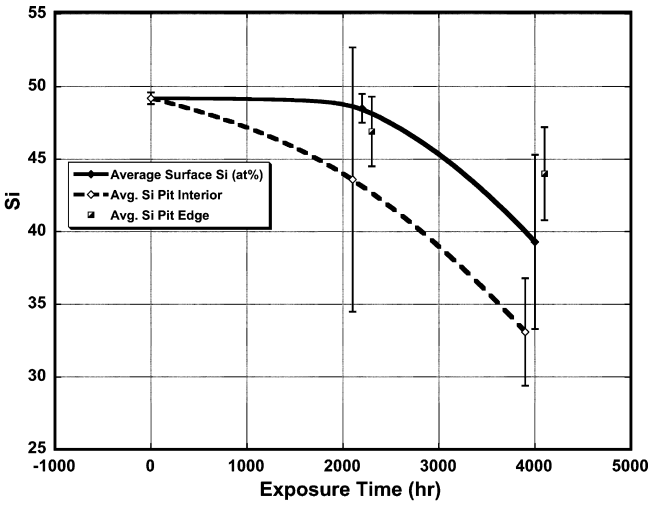

Fig. 5. Plot of average Si composition in at.% as a function of time and location on the surface of the CVD SiC after 2200 h and 4000 h exposures. The average Si content on the surface decreases relative to C but for the pit interiors the Si decrease is greater. The data points have been shifted slightly along the *x*-axis (time) for clarity.

773 K and observed approximately linear mass loss that was slower than that reported by Kim et al. under static conditions at 633 K. They attributed this reduced corrosion rate compared to Kim et al. to the careful control of oxygen to the part per billion level, which was hypothesized to reduce corrosion rates. They also observed preferential grain boundary attack of the SiC surface and an overall loss of Si at the surface as measured using Auger electron spectroscopy (AES). Again, loss of Si was attributed to formation of soluble silicon hydroxides. SEM of the surface revealed clear grain boundary attack in the 773 K flowing water.

In contrast to the foregoing, the formation of pits on β-SiC is a new observation during corrosion in deoxygenated water at 573 K keeping in mind that the current study considered exposure times about a factor of 10 longer than any of the previous studies. As discussed below, there are several explanations that can account for their formation on the surface but the majority of the theory and knowledge of corrosion of SiC in water supports a more general and uniform dissolution of SiC by removal of Si in the form of water-soluble hydroxides. The appearance of the pits in this study, while quite interesting, would seem to be a transient phenomenon and the SiC–water system moves toward a more uniform equilibrium state as shown by the data following the re-exposure of the pitted samples, which shows the pits disappearing with increasing corrosion.

The observation of pitting corrosion in SiC materials for high-temperature corrosion processes, $T > 1273$ K, has been documented for molten salts [27,28] but no literature exists, to the best of our knowledge, for pit formation in pure water at 573 K [16–19]. However, there are reaction mechanisms that could account for the formation of pits in β-SiC at any temperature [17,29]. Pits are formed due to inhomogeneous corrosion processes either associated with impurities or inclusions, grain boundaries with chemical segregations, or specific electrochemical conditions where a localized corrosion cell is formed. Although the purity of the β-SiC used in this study is quite high, impurities cannot be ruled out as the source of the observed pitting except that no specific impurity is associated with the observations made here. Rather, the explanation of the pit formation is better described by local galvanic cell formation due to hydrolysis reactions involving dissolution of silica and formation of carbon. However, the observations in Fig. 3 demonstrate the importance of grain boundaries or crystallography on the initial corrosion events.

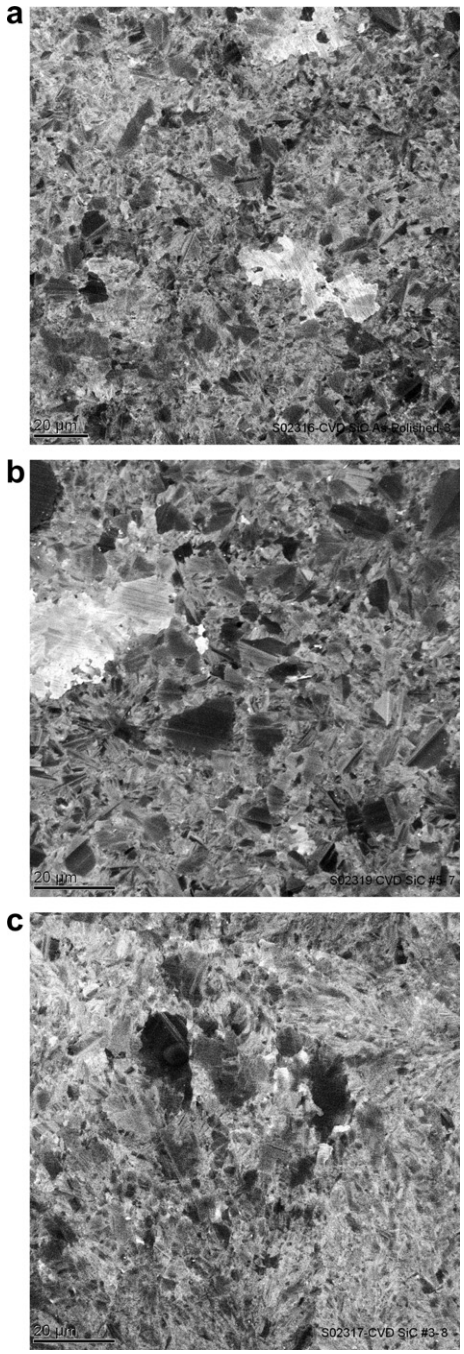

Fig. 6. SEM micrographs of typical surface regions for (a) as-polished, (b) 3600 h exposure and (c) 5400 h exposure specimens. The grain structure that is visible in (a) and (b) is distorted in (c) and the surface appears more distorted in (c).

Several groups have studied hydrothermal corrosion of carbide and nitride ceramics [8,17,29] and the following reactions between SiC and water have been shown to be thermodynamically possible

$$SiC + 2H_2O \rightarrow SiO_2 + CH_4, \quad (1a)$$

$$SiC + 4H_2O \rightarrow SiO_2 + CO_2 + 4H_2, \quad (1b)$$

$$SiC + 3H_2O \rightarrow SiO_2 + CO + 3H_2, \quad (1c)$$

$$SiC + 4H_2O \rightarrow Si(OH)_4 + CH_4. \quad (1d)$$

These reactions all act to form silica on the surface of the SiC except for 1(d) that forms silicon hydroxide. Although these are important

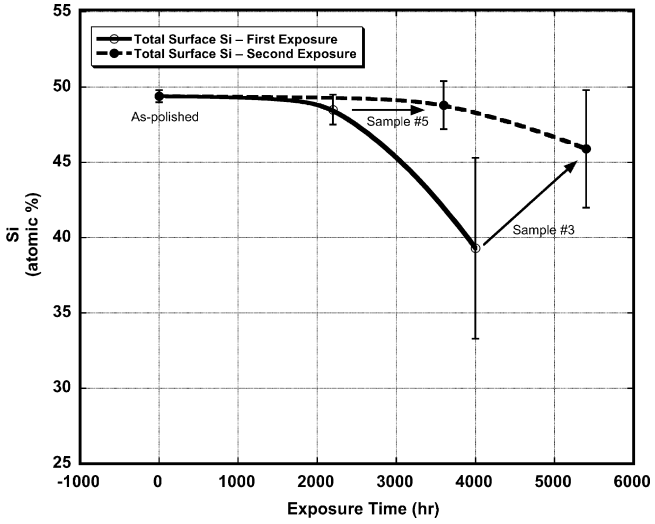

Fig. 7. Total surface concentration of Si in at.% measured using quantitative EDS methods in the SEM for all samples. Open circles indicate first exposure testing results and closed circles are second exposure testing. The arrows indicate how each sample shifted in surface composition after repeated exposures.

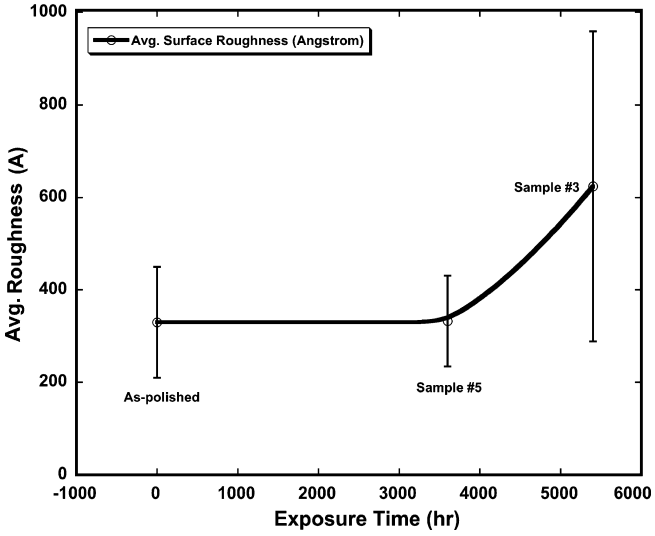

Fig. 8. Average arithmetic surface roughness (Ra) data obtained on exposed samples using a stylus profilometer and an average of six scans per sample.

reactions for protection of SiC in aggressive environments, the further corrosion of SiC depends sensitively on the protectiveness of the outer silica layer. In water, unfortunately, this layer is not protective even at 573 K and 10 MPa. Tomozawa and co-workers have shown in detail how silica reacts with and intermixes with water under these conditions [20–24], building on the work of Doremus [25]. Water readily bonds with silica, diffuses into silica, and causes structural changes that act to reduce its protectiveness. Far worse than this, however, is the dissolution of silica into water, or at higher temperatures into water vapor, via the formation of soluble or volatile silicon hydroxides.

The dissolution of the surface silica allows further reactions between water and SiC to occur without the limiting steps of diffusion. The following dissolution reactions can occur depending on the oxygen activity and pH in the water

$$SiO_2 + H_2O \rightarrow H_2SiO_3^- + H^+ \rightarrow SiO_3^{2-} + 2H^+ \quad (2)$$

If SiC reacts with water to form $Si(OH)_4$ via reaction (1d), which is an appropriate reaction for SiC in de-oxygenated water, then dissolution of the hydroxide can occur as

$$Si(OH)_4 \rightarrow H_3SiO_4^- + H^+ \rightarrow H_2SiO_4^{2-} + 2H^+. \quad (3)$$

In this case, no protective silica layer forms and the rate of dissolution depends on the pH of the water. Even in neutral pH water these reactions occur and lead to non-protective corrosion of SiC, albeit with sluggish kinetics that are most likely linear in time.

The data obtained in this exposure did not permit highly accurate weight gain measurements since large monolithic blocks of β-SiC were exposed, which provides the least possible surface area for exposures in contrast to those that used SiC powders. In addition, no IR or Raman data were obtained to explore surface chemistry changes after long-term exposures. However, the smooth polished surfaces allowed us to image surface morphology changes after the exposures and observe the formation of the pits. Reactions (2) and (3) both suggest that localized corrosion cells are possible based on simple hydrolysis reactions and requisite charge transfer. In this case, the pits result from a local increase in silica dissolution rates leading to increased loss of silicon from the SiC and the loss of carbon either via CO, CO_2, or CH_4. Alternatively, the deposition of carbon as has been observed in the hydrothermal corrosion of Tyranno SiC fibers [29] via

$$CO_2 + CH_4 \rightarrow 2C + 2H_2O. \quad (4)$$

This reaction, if it occurred, would deposit a thin film of carbon on the SiC surface. Although this experiment did not include any detailed surface analysis, the data obtained here are consistent with either a loss of silica and/or deposition of carbon.

The EDS data obtained in Fig. 4 are typical of all the large pits that were imaged in this study. This data, which shows enhanced carbon and oxygen with decreased silicon, is more consistent with the formation of silica on the surface plus a gradual loss of silica through hydrolysis. Otherwise, the enhanced oxygen signal cannot be accounted for and the enhanced carbon only makes sense in this case due to a local loss of silicon. This suggests that the operative reactions are Eqs. (1a), (1b), (1c) and not Eq. (1d) so that SiO_2 is produced but is then lost due to hydrolysis reaction such as Eq. (2).

The complex structure of the pits is quite remarkable and deserves some comment. Jacobsen and Smialek observed pit or cavity formation at elevated temperatures on the surface of SiC that was accounted for by the formation of gas bubbles [27]. The formation of the small pits on the surface in this study, such as those shown in Fig. 3(d) and that are submicron in size, could be due to the formation of volatile carbon species, such as CO, CO_2, or CH_4 that act to disrupt the surface silica layer. In the high-pressure water of this study, this silica layer is saturated with water and would be easily disrupted by gaseous reaction products. Locally, the CO and CO_2 would increase the acidity and accelerate the corrosion process, perhaps resulting in the formation of the local pits due to the agglomeration of the small pits into larger electrochemical cells on the surface. The preferential formation of bubbles or localized corrosion along grain boundaries or aligned within grains as shown in Fig. 3(f) is due to higher dissolution rates at boundaries or along certain preferred crystallographic orientations.

The use of fractals and the mathematics of fractals in analysis of pit growth is widely used and accepted [30–33]. In general, pitting can be treated as a stochastic process in terms of initial formation of localized areas of defected protective films; that is that pits form randomly on the surface. However, once a pit nucleates then local changes due to the corrosion process dictate the resulting pit growth rate and growth process. The pits observed here certainly have the visual appearance of self-similarity that has been observed in other materials [31]. A Monte Carlo model of pitting in

aluminum alloys suggests that the pit growth observed here can be characterized as stable pit growth or smooth radial pit growth outward from an initial pit embryo [32]. The pits observed here appear to have grown from the cooperative agglomeration of many thousands of smaller radial pits such that a general smooth radial pit results. The fractal nature of the pit is then related to the cooperative growth of the smaller pits and their eventual merger into larger and larger corroded regions.

It is then hypothesized to be the case that the pits are a transient phenomenon and give way to a more uniform surface corrosion as evidenced by their disappearance following the additional 1400 h re-exposure to identical deoxygenated water at 573 K. However, it may be that some slight chemistry change occurred in the water chemistry so that the absolute stability of the pits cannot be completely ruled out. The end result of the water exposure is perhaps best understood in the data shown in Fig. 7 showing the gradual loss of Si due to hydrolysis reactions such as those discussed in Eqs. (1) and (2) above. More study would be needed to determine the absolute rate kinetics of this loss and the exact determination of the mass loss was not made here, although it is small. The results observed here are consistent with reduced corrosion rates in water with low oxygen concentrations compared with studies in water without oxygen control as also observed by others [16–19].

However, the use of SiC-based materials in water-cooled reactors appears to have some concerns associated with the corrosion mechanisms discussed here. The swelling at 573 K is significant and the localized corrosion problem is more than worrisome. SiC-based nuclear fuel pellets as suggested by Ref. [2] do not appear to be sound and technically feasible based on these results. This is especially significant since the small fuel pellets have only a thin SiC coating that acts as a primary fuel-cladding layer. That layer cannot be compromised by pitting or grain boundary corrosion and remain a successful cladding layer, nor can it be compromised by Si dissolution in water. SiC fuel rods based on SiC tubes with thicker walls likely would have enough thickness to survive adequate exposure lifetimes unless localized corrosion dominated compared to uniform corrosion. Significant Si loss from the surface in this study is documented in only hundreds or thousands of hours compared to the several years a SiC fuel rod or pellet would be expected to survive in a reactor.

5. Conclusions

The use of β-SiC materials in water-cooled reactors is brought into question by the corrosion results presented here that documents for the first time pitting of SiC exposed to pure water at 573 K. Small pits form within 2000 h of exposure to 573 K deoxygenated water and coalesce into much larger pits by 4000 h. The nature and structure of the pits, together with their chemistry, demonstrates that Si dissolution in the form of water-soluble silicon hydroxides is occurring. The Si dissolution becomes inhomogeneous and sets up localized galvanic reactions that readily form large surface pits. In the pits Si is depleted and C is enhanced relative to the average surface compositions. Gradually the pits give way to a more uniform surface corrosion of the SiC with depletion of Si on the order of a few atomic percent measured in slightly over 5000 h exposure times. This is in qualitative agreement with the findings of others studying the exposure of β-SiC to high-temperature, high-pressure water, even with oxygen concentrations in the parts per billion levels.

Acknowledgement

PNNL is operated for the US Department of Energy by Battelle Memorial Institute under Contract DE-AC06-76RLO 1830.

References

[1] G.A. Filippov, E.I. Grishanin, L.N. Fal'kovskii, B.I. Fonarev, P.N. Alekseev, N.E. Kukharkin, P.A. Fomichenko, V.F. Tsibul'skii, A.V. Chibinyaev, Atom. Energy (Atomnaya Energiya) 100 (2006) 197.
[2] N.N. Ponomarev-Stepnoi, N.E. Kukharkin, A.A. Khrulev, Y.G. Degal'tsev, E.S. Glushkov, G.A. Filippov, E.I. Grishanin, L.N. Fal'kovskii, Atom. Energy (Atomnaya Energiya) 86 (1999) 443.
[3] Y. Katoh, T. Nozawa, L.L. Snead, T. Hinoki, A. Kohyama, Fus. Eng. Design 81 (2006) 937.
[4] M. Gasparotto, R. Andreani, L.V. Boccaccini, A. Cardella, G. Federici, L. Giancarli, G. Le Marois, D. Maisonnier, S. Malang, A. Moeslang, Y. Poitevin, B. van der Schaaf, M. Victoria, Fus. Eng. Design 66–68 (2003) 129.
[5] T. Muroga, M. Gasparotto, S.J. Zinkle, Fus. Eng. Design 61–62 (2002) 13.
[6] S.J. Zinkle, N.M. Ghoniem, Fus. Eng. Design 51–52 (2000) 55.
[7] Y. Katoh, L.L. Snead, C.H. Henager Jr, A. Hasegawa, A. Kohyama, B. Riccardi, H. Hegeman, J. Nucl. Mater. 367–370A (2007) 659.
[8] N. Jacobson, D. Myers, E. Opila, E. Copland, J. Phys. Chem. Solid 66 (2005) 471.
[9] Q.N. Nguyen, E.J. Opila, R.C. Robinson, J. Electrochem. Soc. 151 (2004) 558.
[10] E.J. Opila, J. Am. Ceram. Soc. 86 (2003) 1238.
[11] E.J. Opila, J. Am. Ceram. Soc. 82 (1999) 625.
[12] E.J. Opila, R.E. Hann Jr., J. Am. Ceram. Soc. 80 (1997) 197.
[13] E.J. Opila, J. Am. Ceram. Soc. 77 (1994) 730.
[14] L.L. Snead, T. Inoki, Y. Katoh, T. Taguchi, R.H. Jones, A. Kohyama, N. Igawa, Advances in Science and Technology 33 (10th International Ceramics Congress 2002, Part D) (2003) 129.
[15] R.H. Jones, L. Giancarli, A. Hasegawa, Y. Katoh, A. Kohyama, B. Riccardi, L.L. Snead, W.J. Weber, J. Nucl. Mater. 307–311 (2002) 1057.
[16] W.-J. Kim, H.S. Hwang, J.Y. Park, W.-S. Ryu, J. Mater. Sci. Lett. 22 (2003) 581.
[17] H. Hirayama, T. Kawakubo, A. Goto, T. Kaneko, J. Am. Ceram. Soc. 72 (1989) 2049.
[18] E. Barringer, Z. Faiztompkins, H. Feinroth, T. Allen, M. Lance, H. Meyer, L. Walker, E. Lara-Curzio, J. Am. Ceram. Soc. 90 (2007) 315.
[19] W.-J. Kim, H.S. Hwang, J.Y. Park, J. Mater. Sci. Lett. 21 (2002) 733.
[20] M. Tomozawa, D.L. Kim, A. Agarwal, K.M. Davis, J. Non-Cryst. Solid 288 (2001) 73.
[21] M. Tomozawa, K.M. Davis, Mater. Sci. Eng. A: Struct. Mater.: Properties Microstruct. Process. 272 (1999) 114.
[22] M. Tomozawa, Phys. Chem. Glasses 39 (1998) 65.
[23] K.M. Davis, M. Tomozawa, J. Non-Cryst. Solid 185 (1995) 203.
[24] H. Wakabayashi, M. Tomozawa, J. Am. Ceram. Soc. 72 (1989) 1850.
[25] R.H. Doremus, J. Non-Cryst. Solid 55 (1983) 143.
[26] A. Abe, H. Tobita, N. Nagata, K. Dozaki, H. Takiguchi, Nucl. Sci. Eng. 149 (2005) 312.
[27] N.S. Jacobson, J.L. Smialek, J. Electrochem. Soc. 133 (1986) 2615.
[28] N.S. Jacobson, J.L. Smialek, J. Am. Ceram. Soc. 68 (1985) 432.
[29] Y.G. Gogotsi, M. Yoshimura, J. Am. Ceram. Soc. 78 (1995) 1439.
[30] J.-J. Park, S.-I. Pyun, Corros. Sci. 46 (2004) 285.
[31] J.-J. Park, S.-I. Pyun, Corros. Sci. 45 (2003) 995.
[32] M. Pagitsas, A. Diamantopoulou, D. Sazou, Chaos Soliton. Fract. 17 (2003) 263.
[33] J.M. Costa, F. Sagues, M. Vilarrasa, Corros. Sci. 32 (1991) 665.